Surface Science 754 (2025) 122688

Contents lists available at ScienceDirect

Surface Science

journal homepage: www.elsevier.com/locate/susc

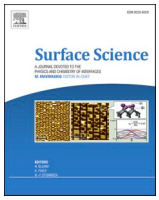

Hydrogen complexes on single-atom alloys: A combined DFT – Kinetic Monte Carlo study

Emanuel Colombi Manzi [a], Michail Stamatakis [b], Giovanni Di Liberto [a,*], Gianfranco Pacchioni [a,*]

[a] Dipartimento di Scienza dei Materiali, Università di Milano - Bicocca, via R. Cozzi 55, 20125 Milano, Italy
[b] Physical and theoretical chemistry laboratory, University of Oxford, S Parks Rd, Oxford OX1 3QZ, United Kingdom

ARTICLE INFO

Keywords:
Single atom alloys
Hydrogen adsorption
Dihydrogen complexes
Density functional theory
Kinetic Monte Carlo

ABSTRACT

Single-Atom Catalysts (SACs) are a new class of solid catalysts with potential applications in a wide spectrum of chemical reactions. The family of Single Atom Alloys (SAAs) is promising for hydrogen-related reactions. One interesting aspect of SACs is that their chemistry is reminiscent of coordination chemistry, and a pertinent example is the formation of dihydrogen complexes in hydrogen-related reactions with similarities to coordination compounds. The formation of these hydrogen complexes has been suggested also for SAAs, based on density functional theory (DFT) calculations. In this work, we conducted a study combining DFT with Kinetic Monte Carlo (KMC) to investigate the formation of hydrogen complexes on a set of SAAs. We scrutinized 14 SAAs with DFT and performed KMC simulations on three relevant cases. Our study considers explicitly the kinetic barriers for the formation and decomposition of these complexes to elucidate the kinetics of the adsorption of molecular H_2 on SAAs. The results indicate that the new species can be relevant depending both on their stability and the reaction barriers involved. In particular, we focused on three test cases, Co@Rh(111), Pd@Rh(111) and Co@Au (111) showing that the formation of dihydrogen species, H_2*, where * indicates an adsorbed complex, can affect the formation of the complex from molecular H_2.

1. Introduction

The attention toward catalysis is steadily increasing, because of the need for improving the activity for key reactions and the overall sustainability of chemical processes [1]. Among key reactions, those involving hydrogen, such as hydrogenations, play a crucial role in various synthesis processes [2–4]. At the same time, the electrochemical evolution of hydrogen from water is attracting significant focus, because it opens the way to produce an energy vector with, in principle, green energy [5–7]. The catalysts for hydrogen-related reactions typically consist of noble and critical metals, such as Pd and Pt [8–13].

Single-Atom Catalysis is emerging as a bridge between homogeneous and heterogeneous catalysis [14,15], with promising applications encompassing, among others, hydrogen related reactions [16–19]. A single-atom catalyst (SAC) is a paradigm of single-site isolation, where a transition metal atom is atomically dispersed in a solid matrix [20–24]. Single-Atom Alloys (SAAs) are a specific family, where transition metal atoms are atomically dispersed on the surface of a host metal [25–29]. They have been introduced about one decade ago with the pioneering work of Sykes and co-workers [27,30–33]. They were successfully applied for hydrogenations, and a large number of studies is proposing SAAs for hydrogen evolution as well [34–36].

On some metals, the interaction of molecular hydrogen with the surface is associated with the breaking of the H—H bond, leading to adsorbed hydrogen atoms (H*) with a mobility that depends on the diffusion barrier [13,37]. However, in analogy with organometallic compounds, SACs can form dihydrogen complexes (H_2*) where the molecule binds to the metal atom and gets activated to some extent, with an elongation of the H—H bond [38–44]. Depending on the extent of the H—H bond activation, the resulting species are classified as dihydrogen, H_2*, or dihydride, H*H*, complexes. Recently, we have adopted density functional theory (DFT) calculations to show that hydrogen complexes can form on SAAs [45]. An important aspect, still not addressed in the literature, is the role of these species on the kinetics of hydrogen adsorptions with formation of complexes on SAA surfaces, a process that is influenced by the reaction barriers of H_2* formation and decomposition

* Corresponding authors.
E-mail addresses: giovanni.diliberto@unimib.it (G. Di Liberto), gianfranco.pacchioni@unimib.it (G. Pacchioni).

https://doi.org/10.1016/j.susc.2024.122688
Received 31 October 2024; Received in revised form 18 December 2024; Accepted 20 December 2024
Available online 1 January 2025

towards H*, as well as the possible spillover of these species from the dopant to the host sites.

To address this point, we designed a study where DFT calculations are combined with the Kinetic Monte Carlo (KMC) approach [46–50], and elucidated the aforementioned processes in 14 SAAs made by seven transition metals (Co, Ni, Cu, Pd, Ag, Ir, Pt) supported on two bulk metal surfaces, Rh(111) and Au(111). The different transition metal atoms were chosen in order to show a broad spectrum of reactivity with hydrogen [45], while the two surfaces have completely different chemical reactivity: Rh(111) is reactive towards H_2 decomposition, and Au(111) is nearly inert [13,37] For comparison, we also investigated H_2 adsorption on the pristine metal surfaces.

Our results showed that on Rh(111) H_2* is a transient species. We selected three relevant test cases, Co@Rh(111), Pd@Rh(111), and Co@Au(111), and performed KMC simulations out of the simulation of hydrogen adsorption, complexes formation and bond breaking with DFT of all 14 SAAs. The results provide different scenarios for H_2 adsorption and evolution.

This study provides an atomistic description of the interaction of H_2 with SAAs, providing further evidence of the relevance of H_2 complexes when considering both thermodynamics (DFT) and kinetics (KMC). The results also provide an example of the complexity of the chemistry of H_2 on single-site catalysts, in which H_2* and H* species can interact with both the dopant as well as the surrounding (host) metal, and there may be competition between the pertinent adsorption and spillover pathways.

2. Computational details

DFT calculations were performed by means of the VASP package [51–53], with the Perdew-Burke-Ernzherof (PBE) functional [54]. The core electrons were described by Plane Augmented Wave (PAW) [55,56] potentials and the valence electrons were described by plane waves with a kinetic energy cut-off of 400 eV. The convergence criteria for electronic and ionic loops were set to 10^{-5} eV and 10^{-2} eV/Å respectively. The sampling of the reciprocal space was done by adopting a grid according to the size of the simulation cell, as done in a previous work by some of us [45] We used the Nudged Elastic Band (NEB) method with the Climbing Image implementation to locate transition states [57]. For the NEB calculations, four images were generated to search for the transition state, and the convergence setup is consistent with that selected for the optimization calculations. Vibrational analysis was performed to check for the existence of only one imaginary frequency to verify that the transition states calculated were indeed first-order saddle points in the potential energy surface. Dispersion terms were included by means of the Grimme's scheme [58]. Indeed, the neglection of dispersion interactions is small but not negligible to the formation of H_2 complexes, as can be appreciated by looking at Table S5. Dispersion interactions are of the order of 0.3 eV causing a stabilization of the complex.

Bulk Rh and Au metals were optimized starting from the experimental face centered cubic crystal structures [59] The calculated lattice parameter *a* was 3.793 Å for Rh and 4.103 Å for Au, in good agreement with the experimental values of 3.796 Å and 4.070 Å, respectively [59]. Five-layers-thick slab models were created from the bulk structures by cleaving along the (111) direction. The atomic coordinates were relaxed by fixing the bottom two layers. The *a, b*, and γ lattice vectors of each system are reported in Table S1 of the Supplementary Information (SI). A vacuum layer of 40 Å was added along the non-periodic direction to avoid spurious effects arising from the interaction between periodic replicas of the system. 14 SAAs models were then created by replacing one atom of Rh or Au with seven different host species, Co, Ni, Cu, Pd, Ag, Ir, Pt. Fig. 1 shows a representative model structure. The binding energy of the metal atoms to the support can be used as a proxy of the stability of the system. However, one must consider that the determination of the catalyst in working conditions is a complex task as it requires to include several aspects such as dissolution of the active phase in the reaction environment, aggregation of the dopant metal atoms and migration to the bulk of the support [60]. These aspects are not investigated in this work as their assessment goes beyond the purpose of this study. The calculated binding energies are in line with those of other systems made by transition metal atoms embedded in carbonaceous materials [61].

Ab-initio thermodynamics was used to evaluate free energy diagrams, where entropic and zero-point energy (ΔE_{ZPE}) contributions were added to the DFT reaction energies (ΔE_{ads}). The entropy of gas phase species was taken from the NIST database and that of solids was neglected. Adsorption energies (ΔE_{ads}) were calculated with respect to the isolated H_2 molecule and the SAA.

KMC simulations were performed by means of the *Zacros* code, which implements the graph-theoretical KMC framework [48,62] Rate constants (k_{TST}) for adsorption, desorption and surface diffusion were calculated according to transition state theory (TST), Eq. (1).

$$k_{TST} = \kappa \frac{k_b \cdot T}{h} \cdot \frac{q^{\ddagger}}{q_{react}} \cdot exp\left(-\frac{E^{\ddagger}}{k_B \cdot T} \right) \quad (1)$$

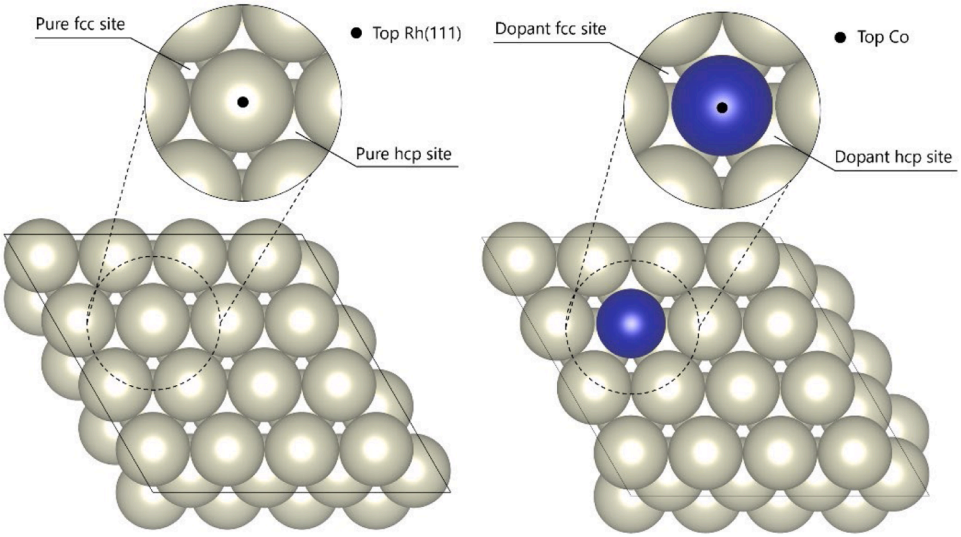

Fig. 1. Graphical representation of the DFT calculation cells used in this study for the pristine Rh(111) surface and for the Co@Rh(111) SAA.

Where k_B is the Boltzmann constant, h is Planck's constant, T the temperature, $q^{\ddagger}$ and q_{react} are the molecular quasi-partition functions for the transition state and the initial state (reactants), respectively. $E^{\ddagger}$ is the activation barrier. κ is the transmission coefficient, which is considered equal 1 for the simulations [63]. We accounted for lateral interactions by employing the Cluster Expansion Hamiltonian (CEH) model implemented in Zacros, which decomposes lattice energy into single-body, two-body, and possibly many-body interactions. This approach allows to calculate activation energies while considering the influence of neighbouring adsorbed species through Brønsted–Evans–Polanyi (BEP) relations, ensuring an accurate representation of the local reaction environment's effects on reaction rates [49].

The calculation of rate constants is done considering the set of equations reported in Section S2 which specify the calculation of translational, rotational and vibrational quasi-partition functions. For all the KMC simulations, we generated large supercells containing 1600 metal atoms. Temperature and pressure conditions were set at 573.15 K and H_2 partial pressure of 2.00 bar respectively, that are compatible with previous experimental studies of hydrogenation on SAAs [64,65]. The number of dentates of the surface species, specifying the number of sites each species binds to for each surface species is set to 1. The max simulation time is chosen differently for each system considering the nature of the catalyst; however, each system was simulated long enough so as to reach stable coverage of the H* species adsorbed on the lattice.

3. Results

3.1. H_2 adsorption on pristine metal surfaces

We start from the adsorption of H_2 on the pristine Rh(111) and Au (111) metal surfaces. It is known that the two systems show a very different affinity for hydrogen, where the former can activate the molecule [66], while the latter is quite inert [67–69].

Fig. 2a shows the free energy diagrams of hydrogen adsorption on Rh (111). The adsorption/dissociation process is exergonic ($\Delta G = -0.27$ eV) and nearly barrierless. A metastable state forms, corresponding to a dihydrogen intermediate (H_2*) on top of the Rh metal (Fig. 2a). The vibrational analysis confirmed that this structure is indeed a minimum with a H—H stretching frequency equal to 2280 cm^{-1}, which is much lower than the corresponding frequency value in the isolated (gas phase) molecule, 4401 cm^{-1}. A previous study indicated that there is correlation between the decrease in the stretching frequency and the H—H bond elongation [42]. Indeed, the calculated H—H distance is 0.94 Å, much larger than in the free molecule, 0.74 Å. The breaking of the H—H bond and the formation of two separated adsorbed hydrogen atoms (2H*) is energetically favourable and requires a negligible activation energy. This implies that H_2* is a transient species on Rh(111).

The two adsorbed hydrogen atoms in the final state can adopt different possible configurations. Here, we considered three site-type combinations (Fig. 2a); the $2H^*_{fcc\text{-}fcc}$ and the $2H^*_{hcp\text{-}hcp}$ ones are nearly isoenergetic while the $2H^*_{hcp\text{-}fcc}$ is less stable by about 0.2 eV, due to a repulsive effect between the two hydrogen atoms that are closer in this configuration. Different is the case of Au(111) (Fig. 2b), where the adsorption of H_2 leads to a physisorped species, and the H—H bond breaking has a very large activation energy (1.14 eV). Again, there are three possible configurations for the 2H* intermediates with same energetic ordering reported for Rh (111), but a very positive free energy of formation (Fig. 2b).

We conducted KMC simulations to unveil the role of dihydrogen intermediate (H_2*) on the kinetics of the hydrogen adsorption process on Rh(111) and on Au(111), but the latter catalyst is inert for this process and will not be further discussed. More interesting is the case of Rh (111), for which we set up three different KMC simulations including different levels of approximation for the H_2 adsorption, which leads to different possible pathways for the adsorption mechanism. First, we neglected the formation of the H_2* intermediate, so that hydrogen can directly go from the gas phase, (H_2), to the $2H^*_{fcc\text{-}fcc}$, $2H^*_{fcc\text{-}hcp}$ or $2H^*_{hcp\text{-}hcp}$ structures. Second, the formation of adsorbed hydrogen atoms, $2H^*_{fcc\text{-}fcc}$, $2H^*_{fcc\text{-}hcp}$ or $2H^*_{hcp\text{-}hcp}$ from the H_2 molecule can proceed via formation of the H_2* intermediate. In this second case, H_2 is forced to go through H_2* before dissociating on the surface. In the third and last simulation setup, we considered the possibility for the catalytic model to freely adopt both mechanisms.

The results obtained from the KMC simulations are summarized in Fig. 3. Starting from the first simulation, the adsorption mechanism favours the $2H^*_{fcc\text{-}fcc}$ combination of sites. The average coverage (Θ) for the simulation is 0.45 at the steady state, which means that almost half of the adsorption sites are occupied by H*. In the second simulation, which considers the formation of H_2*, Θ decreases to ~ 0.29. Comparing the coverage of these two simulations with the third case, one can observe that the latter simulation leads to unchanged coverage, Θ ~ 0.30.

3.2. Atomic H* on SAAs

For each SAA, we first studied the adsorption of atomic H* in the proximity of the dopant metal atom, Section S3. For comparison purposes, Table S3 reports the adsorption energy of H* on pristine Rh(111) and Au(111) metal surfaces, while the same adsorption energies, but calculated on host sites of SAAs, are reported in Table S4. The results show that the presence of the guest metal atom affects the energetics of H* adsorption both on the first and the second nearest-neighbor sites of the host metal, in line with a previous study [70]. This clearly indicates that the effect of the guest metal is not restricted to the first neighbors.

In the case of M@Rh(111), the adsorption of H* atoms can occur in different sites. We explored adsorption on top of the dopant atom, in hollow sites between the dopant and the first nearest neighbors, and related structures on the second nearest neighbor host metal atoms,

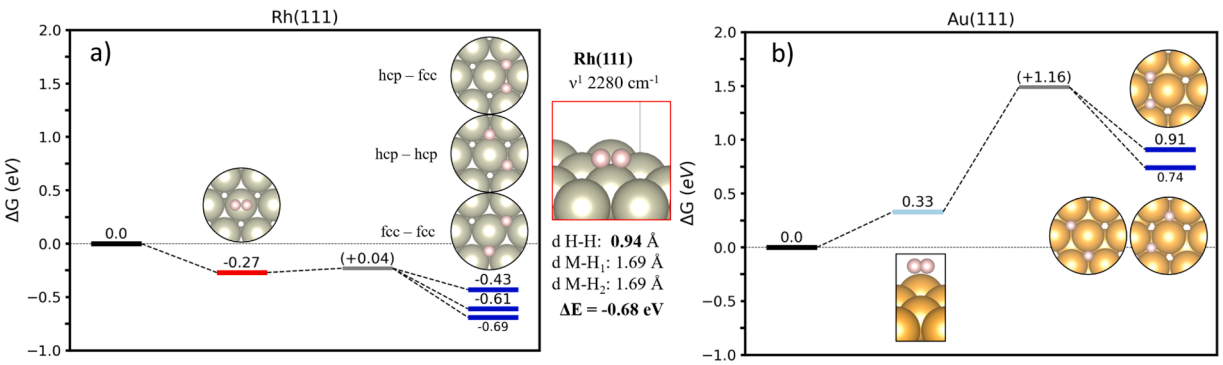

Fig. 2. Free energy diagram of H_2 adsorption on (a) Rh(111), and (b) Au(111). When nearly isoenergetic transition states are present, a single energy value is reported.

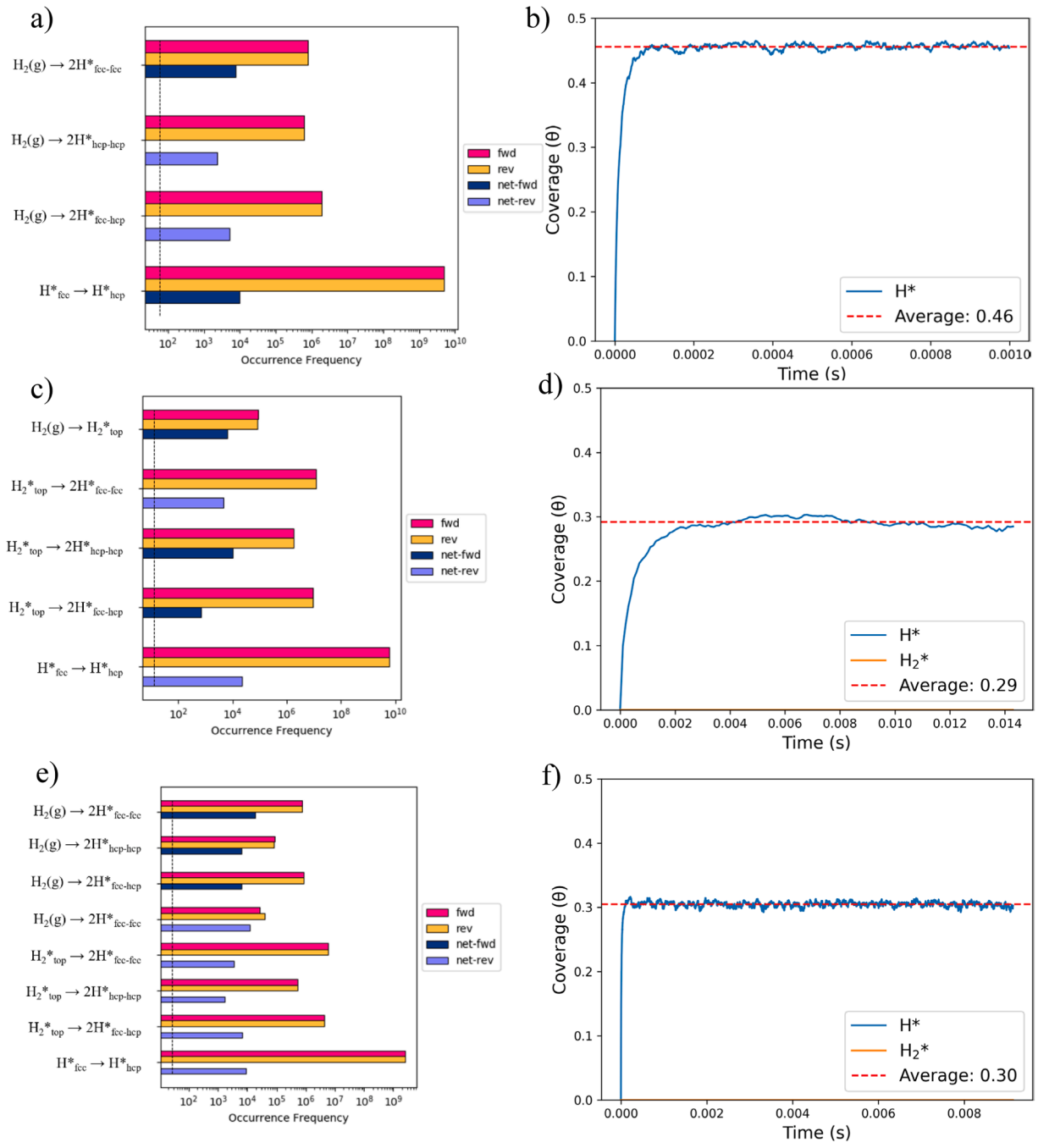

Fig. 3. KMC results for the three simulations performed to model hydrogen adsorption on Rh(111). (a) and (b) are related to the simulation performed considering the mechanism: $H_{2(g)} \rightarrow 2H^*$. (c) and (d) show the KMC simulation results obtained for the mechanism which considers explicitly the formation of the dihydrogen intermediate: $H_{2(g)} \rightarrow H_2{}^* \rightarrow 2H^*$. (e) and (f) show the results of similar simulations, which, however, consider that the system can adopt both mechanisms proposed for the first two simulations.

Table S4. H* can be adsorbed on top of the metal atom (M), and this configuration is the most stable one for Ir@Rh(111). In the most stable adsorption configuration for Co@Rh(111) H* is bound to a hollow site. In the rest of the cases, there are different minimum structures which are nearly isoenergetic, and involve adsorption close to the dopant or in the second nearest neighbor sites. In all cases, the global minimum structure is more stable than the catalyst and 1/2H_2, and therefore the adsorption is exergonic. In the case of Au-based SAAs, the adsorption close to the metal dopant is always more favorable than on Au(111). The formation of H* on Co@Au(111) is favorable, with a ΔG = -0.11 eV, while in the rest of the cases the adsorption of H* is characterized by a positive ΔG.

3.3. *Dihydrogen species, H_2* or H*H*, on SAAs*

We subsequently investigated the adsorption of H_2 on the SAAs under consideration. The formation of the H_2* intermediate was observed on Co@Rh(111), Pd@Rh(111), Co@Au(111) and Ni@Au (111). In the other cases, we observed the formation of a dihydride species, H*H*. All the calculated adsorption free energies of adducts and structural information are reported in Table 1.

We start by discussing Co@Rh(111). The adsorption of H_2 leads to the formation of a dihydrogen intermediate ($\Delta G = -0.20$ eV) with an activation barrier of 0.44 eV, Fig. 4a. Another possible minimum, which is the global minimum energy structure, consists of two separated

Table 1
Calculated adsorption and free energies, H—H and dopant-H distances, for the various adducts formed after H_2 adsorption to the SAA.

System	Intermediate[a]	ΔE / eV	ΔG / eV	$d_{H—H}$ / Å	$d_{M\text{-}H}$ / Å
Rh(111)					
Co@Rh(111)	H_2*	−0.61	−0.20	0.93	1.57
	2H*	−1.16	−0.75	2.59	1.79
Ir@Rh(111)	H*H*	−1.14	−0.73	2.21	1.69
Ni@Rh(111)	2H*	−1.13	−0.72	2.59	1.77
Pd@Rh(111)	H_2*	−0.30	0.11	0.84	1.81
	2H*	−0.99	−0.58	2.99	1.95
Pt@Rh(111)	2H*	−0.89	−0.48	2.72	1.83
Cu@Rh(111)	2H*	−1.03	−0.62	2.98	1.96
Ag@Rh(111)	2H*	−1.00	−0.59	3.68	2.29
Au(111)					
Co@Au(111)	H_2*	−0.58	−0.17	0.91	1.57
	H*H*	−0.42	0.06	2.01	1.56
Ir@Au(111)	H*H*	−1.07	−0.66	1.71	1.60
Ni@Au(111)	H_2*	−0.17	+0.24	0.75	1.66
	H*H*	−0.10	+0.31	2.49	1.69
Pd@Au(111)	H*H*	+0.13	+0.54	2.85	1.85
Pt@Au(111)	H*H*	−0.18	+0.23	2.34	1.66
Cu@Au(111)	H*H*	+0.18	+0.59	2.86	1.90
Ag@Au(111)	2H*	+0.52	+0.93	3.30	1.98
	2H*	+0.29	+0.70	3.64	2.34

[a] H_2* = adsorbed dihydrogen complex; H*H*: adsorbed dihydride complex; 2H*: two separated adsorbed H atoms.

adsorbed H atoms, 2H*, where each H* is adsorbed on a hollow site, with a $\Delta G = -0.75$ eV. The migration of H* species to Rh sites leads to different minima very similar in energy. In all cases, the diffusion barriers are rather small, always below 0.2 eV. On Pd@Rh(111), at variance with the previous case, the dihydrogen complex is less stable than the non-interacting moieties, H_2 and the catalyst, Fig. 4b. Also, the breaking of H—H bond is an activated process with a barrier of 0.41 eV, leading to the formation of a stable dihydride H*H* intermediate that is nearly isoergonic with other adducts resulting from the spillover of hydrogen to the host surface with negligible activation energies. Moving to Co@Au (111) (Fig. 4c), it is not surprising that Co binds hydrogen and that the resulting structure corresponds to the most stable configuration of the adduct. Indeed, we observe the formation of a dihydrogen H_2* species on Co with $\Delta G = -0.17$ eV. The formation of a dihydride H*H* intermediate is less favourable by 0.23 eV, and is associated to a barrier of 0.29 eV. The spillover process is achieved by overcoming a relatively large activation energy of 0.50 eV. Finally, we discuss Ni@Au(111). The hydrogen adsorption on Ni leads to a less stable H_2* intermediate with respect to Co@Au(111), akin to the case of Rh-based SAAs. The molecular adsorption of H_2 as H_2* is endergonic with respect to H_2 and the catalyst, $\Delta G = +0.24$ eV, Fig. 4d. The breaking of the H—H bond to form the H*H* dihydride intermediate is an activated process with a barrier of about 0.4 eV. Also, the spillover process is activated. Since H_2* formation is endergonic on Ni@Au(111), we focused our subsequent calculations to the first three cases, Co@Rh(111), Pd@Rh(111) and Co@Au (111).

For these SAA systems we conducted KMC simulations to study in detail the kinetics of hydrogen adsorption and analyse the role of the dopant atoms on the mechanism of adsorption/desorption of hydrogen, as well as that of the Rh(111) and Au(111) host metal surfaces.

The lattice of Rh(111) based SAAs is modelled by assuming that from the second nearest-neighbor hollow sites onward, the reactivity is equivalent to that of the pure Rh(111) surface sites (labelled as “fcc” and “hcp” sites), since sizeable changes occur only for the first neighboring region, see Fig. 5a. In the case of the Au(111) surface the energetics of adsorption is sensitive up to the second neighbors. For this reason, the lattice incorporates site types appropriate for the 1st and 2nd nearest-neighbor sites, so as to explicitly model the DFT-calculated binding energies of hydrogen species on these sites, which are different than those of the bulk Au surface, Fig. 5b.

Starting from Co@Rh(111), the most probable event, Fig. 6a, is the migration of an adsorbed H atom, H*, on various surface sites, indicating a high mobility of the species. If we compare the occurrence frequency (*i.e.* the number of events occurred divided by the duration of the simulation) for hydrogen adsorption from the gas phase to the H_2* with the dopant or with the host metal, we see that H_2 preferentially binds the surface on Rh sites. In fact, H_2 binds to the Co atom with $\Delta G = -0.20$ eV, and to the Rh atoms of the (111) surface with $\Delta G = -0.27$ eV. The formation of the dihydrogen complex, H_2*, on Co@Rh(111) is activated, with a barrier of 0.44 eV, while H_2* formation on Rh(111) is barrierless. This is an example where the catalytic event occurs on the host metal surface rather than on the metal atom dopant.

Moving to Pd@Rh(111), the adsorption of H_2 on the metal dopant is thermodynamically less favourable than on Co@Rh(111), with a $\Delta G_{H2} = 0.11$ eV. However, on Pd@Rh(111) the process is barrierless, at variance with Co@Rh(111), as previously discussed. This explains why in the occurrence plot, Fig. 6b, the adsorption of H_2, or alternatively its evolution, the host and guest metals are competitive. Similar with the previous case, once H_2 is adsorbed it becomes very mobile on the surface after dissociation.

The last case is Co@Au(111). As discussed above, Au(111) is nearly inert towards molecular hydrogen, and no adsorption events are observed in KMC simulation. The adsorption of H_2 is therefore comparatively more frequent on the dopant site via formation of a dihydrogen complex, Fig. 6c. Once formed, H_2* can evolve to dihydride, H*H*, with a small barrier of 0.12 eV. Co@Au(111) is an example of a catalyst where H_2 adsorption or evolution is expected to occur on the dopant species.

4. Conclusions

In this work we performed a combined DFT and KMC study on a set of single-atom alloys. We focused on the formation of hydrogen complexes and their impact on the kinetics of the process. We first tested the role of hydrogen complexes on the adsorption process on two pristine metal surfaces, Rh(111) and Au(111). On Rh(111), we found that a metastable transient species corresponding to a dihydrogen complex forms. Au(111), on the contrary, is inert towards hydrogen. Then, we considered a set of 14 SAAs, made by seven transition metals atoms (Ir, Co, Ni, Pd, Pt, Cu, Ag) embedded in Rh(111) and Au(111) surfaces. Except for Ni@Rh(111), the remaining systems exhibit minimum energy structures corresponding to a dihydrogen (H_2*) or a dihydride (H*H*) complex. In four cases, Co@Rh(111), Pd@Rh(111), Co@Au(111) and Ni@Au(111), the dihydrogen complex has a formation free energy lower than that of two hydrogen atoms (2H*) adsorbed on the transition metal dopant. Except for Ni@Au(111), the formation of the dihydrogen complex is exergonic. Results for Co@Rh(111), Pd@Rh(111), Co@Au(111) show a wide spectrum of possible effects. In the first case, the dihydrogen complex has a marginal role to the kinetic of the adsorption, that is dominated by adsorption on the host metal. On Pd@Rh(111), the affinity of the guest atom for hydrogen is higher, and the formation of the complex is competitive with the formation of chemisorbed hydrogen species H* on the host metal surface.

In conclusion, the formation of dihydrogen species, H_2*, affects the kinetics of hydrogen adsorption on SAAs. The results provide further insights on the importance of considering the formation of dihydrogen complexes when dealing with hydrogen-related reactions on SAAs.

CRediT authorship contribution statement

Emanuel Colombi Manzi: Investigation, Data curation. **Michail Stamatakis:** Writing – review & editing, Validation, Supervision, Conceptualization. **Giovanni Di Liberto:** Writing – review & editing, Writing – original draft, Supervision, Formal analysis, Conceptualization. **Gianfranco Pacchioni:** Supervision, Conceptualization.

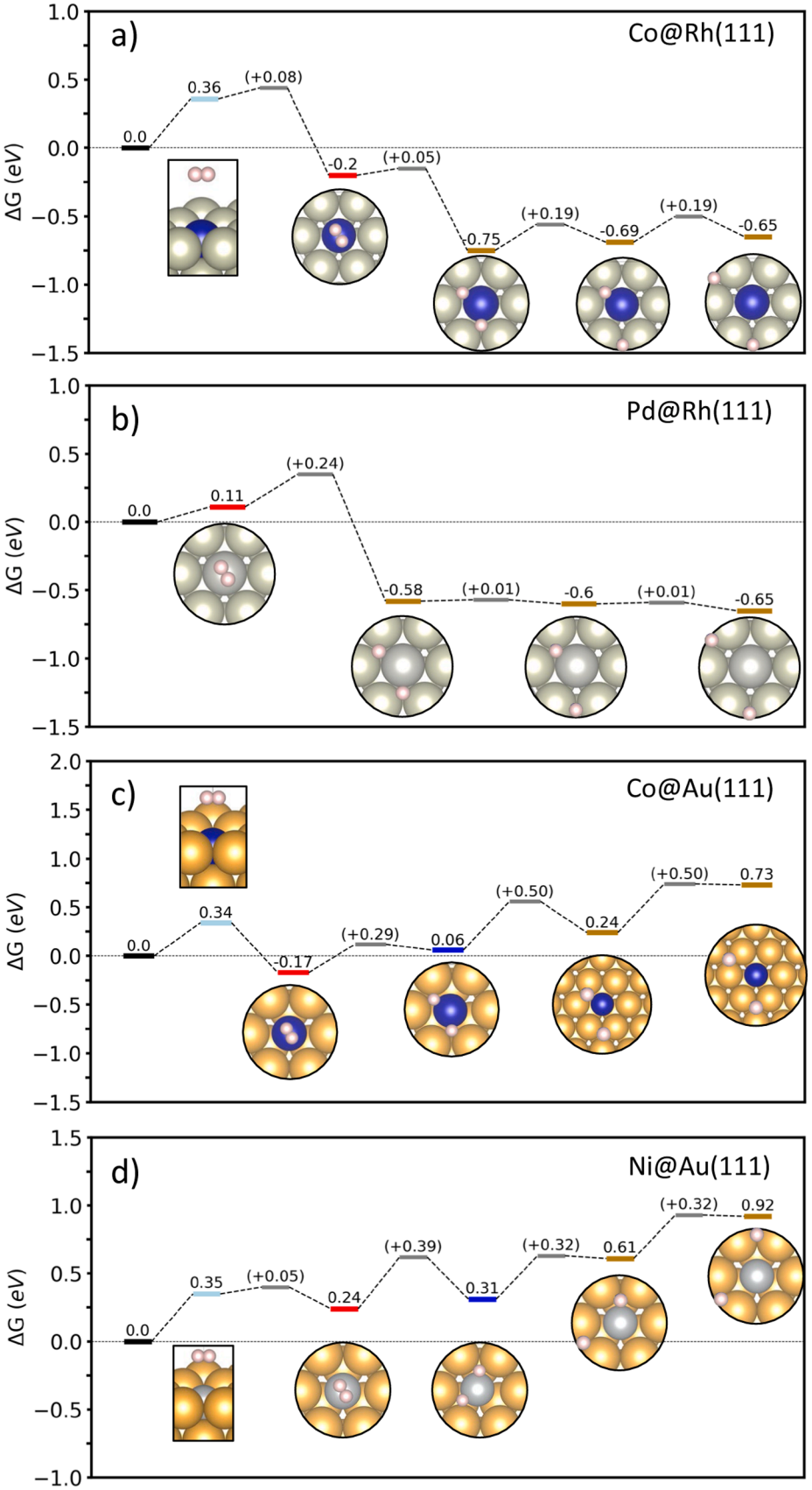

Fig. 4. Free energy diagrams of hydrogen adsorption on a) Co@Rh(111), b) Pd@Rh(111), c) Co@Au(111), d) Ni@Au(111) obtained from DFT calculations. Black: gas-phase H_2; light blue: dihydrogen intermediates (H_2*); red: dihydride intermediates (H*H*); yellow: 2H* intermediates. In gray the transition states (activation energy in brackets).

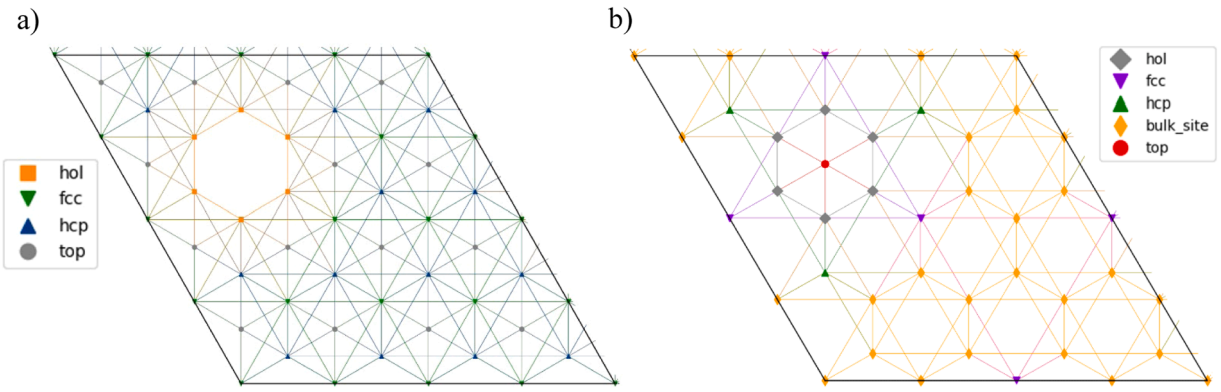

Fig. 5. Kinetic Monte Carlo lattice representation of the surface lattice of SAAs, panel (a) is for M@Rh(111) and panel (b) is for M@Au(111). Panel (a) represents the model for M@Rh(111) Single-Atom Alloys in which the adsorption sites are differentiated in "hol" for the first nearest-neighbor sites around the dopant metal with energetics obtained from DFT calculations on SAAs; "fcc" and "hcp" sites are related to the energetics of pure Rh(111) surface. In the lattice of panel b the M@Au (111) lattice considers explicitly not only the "hol" sites, but also for the second nearest-neighbor sites ("fcc" and "hcp" in purple and green respectively) and the energetics come from DFT calculations of each SAA; for the remaining sites, the energetic parameters are defined from DFT calculations on the pure Au(111) surface.

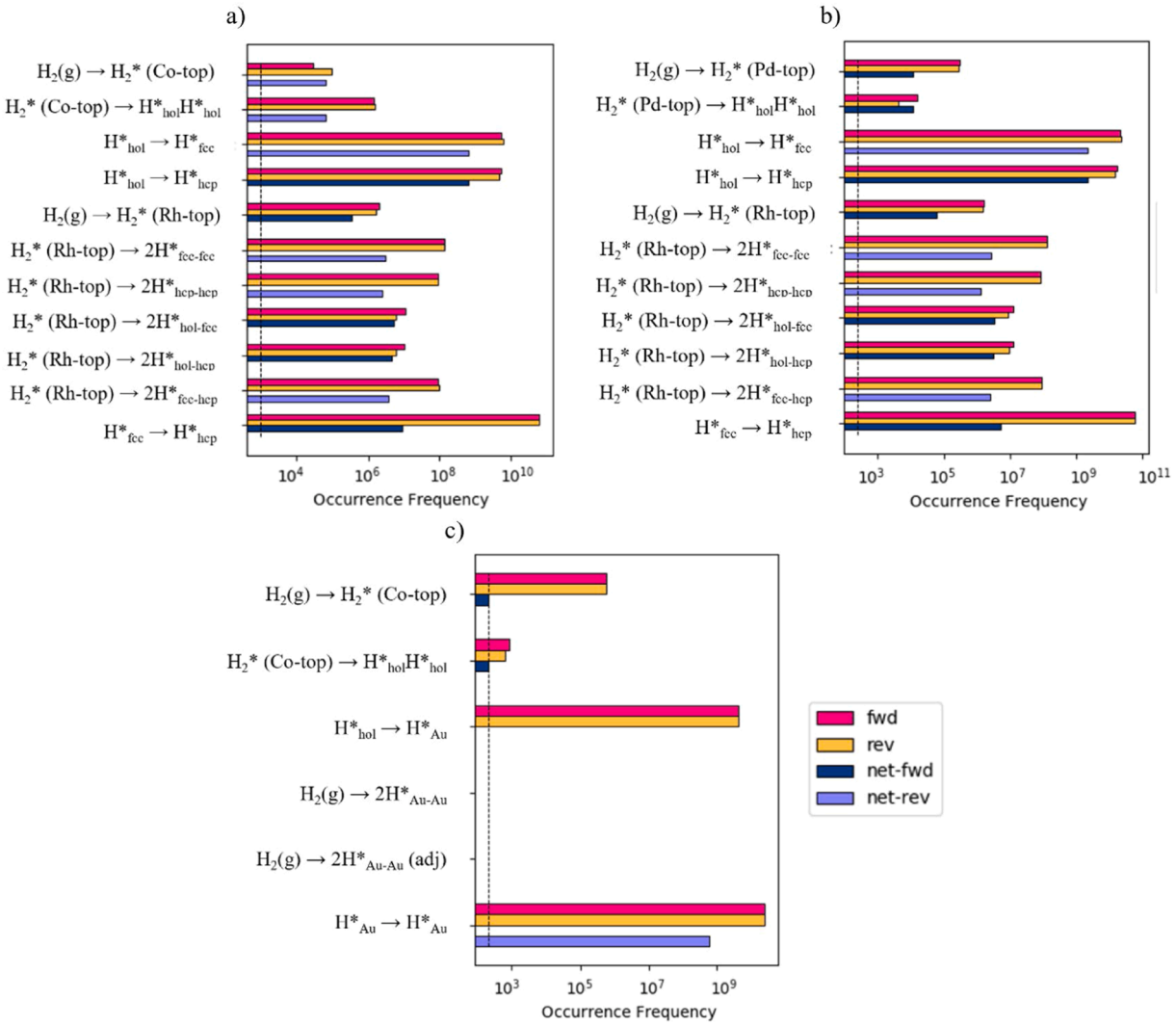

Fig. 6. KMC simulation results obtained for a) Co@Rh(111), b) Pd@Rh(111), c) Co@Au(111).

Declaration of competing interest

The authors declare that they have no known competing financial interests or personal relationships that could have appeared to influence the work reported in this paper.

Acknowledgements

GDL has received funding through the PRIN PNRR project "SAC-toH2" (project code P2022AZETB) by the Italian Ministry for Universities and Research (MUR), in the context of the National Recovery and Resilience Plan and co-financed by the Next Generation EU. We also thank the COST Action 18234 supported by COST (European Cooperation in Science and Technology). We acknowledge EuroHPC Joint Undertaking for awarding us access to LEONARDO at CINECA under the project EHPC-REG-2024R01-071.

Supplementary materials

Supplementary material associated with this article can be found, in the online version, at doi:10.1016/j.susc.2024.122688.

Data availability

The data supporting this work can be obtained upon reasonable request to the authors.

References

[1] G. Centi, J. Čejka, Needs and gaps for catalysis in addressing transitions in chemistry and energy from a sustainability perspective, ChemSusChem. 12 (2019) 621–632, https://doi.org/10.1002/cssc.201802637.
[2] N.B. Johnson, I.C. Lennon, P.H. Moran, J.A. Ramsden, Industrial-scale synthesis and applications of asymmetric hydrogenation catalysts, Acc. Chem. Res. 40 (2007) 1291–1299, https://doi.org/10.1021/ar700114k.
[3] W. Lubitz, W. Tumas, Hydrogen: An Overview, Chem. Rev. 107 (2007) 3900–3903, https://doi.org/10.1021/cr050200z.
[4] X. Li, Y. Yan, X. Zheng, Y. Yao, Y. Liu, Atomically dispersed V-N-C catalyst with saturated coordination effect for boosting electrochemical oxygen reduction, Chemical Engineering Journal 444 (2022) 136363, https://doi.org/10.1016/j.cej.2022.136363.
[5] G. Zhao, K. Rui, S.X. Dou, W. Sun, Heterostructures for electrochemical hydrogen evolution reaction: a review, Adv. Funct. Mater. 28 (2018) 1803291, https://doi.org/10.1002/adfm.201803291.
[6] M.Z. Rahman, M.G. Kibria, C.B. Mullins, Metal-free photocatalysts for hydrogen evolution, Chem. Soc. Rev. 49 (2020) 1887–1931, https://doi.org/10.1039/C9CS00313D.
[7] X. Zou, Y. Zhang, Noble metal-free hydrogen evolution catalysts for water splitting, Chem. Soc. Rev. 44 (2015) 5148–5180, https://doi.org/10.1039/c4cs00448e.
[8] G. Vilé, D. Albani, M. Nachtegaal, Z. Chen, D. Dontsova, M. Antonietti, N. López, J. Pérez-Ramírez, A Stable Single-Site Palladium Catalyst for Hydrogenations, Angewandte Chemie International Edition 54 (2015) 11265–11269, https://doi.org/10.1002/anie.201505073.
[9] D. Albani, G. Vilé, S. Mitchell, P.T. Witte, N. Almora-Barrios, R. Verel, N. López, J. Pérez-Ramírez, Ligand ordering determines the catalytic response of hybrid palladium nanoparticles in hydrogenation, Catal. Sci. Technol. 6 (2016) 1621–1631, https://doi.org/10.1039/C5CY01921D.
[10] M. Crespo-Quesada, A. Yarulin, M. Jin, Y. Xia, L. Kiwi-Minsker, Structure sensitivity of Alkynol hydrogenation on shape- and size-controlled palladium nanocrystals: which sites are most active and selective? J. Am. Chem. Soc. 133 (2011) 12787–12794, https://doi.org/10.1021/ja204557m.
[11] N.M. Marković, B.N. Grgur, P.N. Ross, Temperature-Dependent Hydrogen Electrochemistry on Platinum Low-Index Single-Crystal Surfaces in Acid Solutions, J. Phys. Chem. B 101 (1997) 5405–5413, https://doi.org/10.1021/jp970930d.
[12] S. Trasatti, Work function, electronegativity, and electrochemical behaviour of metals, J. Electroanal. Chem. Interfacial. Electrochem. 39 (1972) 163–184, https://doi.org/10.1016/S0022-0728(72)80485-6.
[13] J.K. Nørskov, T. Bligaard, A. Logadottir, J.R. Kitchin, J.G. Chen, S. Pandelov, U. Stimming, Trends in the Exchange Current for Hydrogen Evolution, J. Electrochem. Soc. 152 (2005) J23, https://doi.org/10.1149/1.1856988.
[14] F. Chen, X. Jiang, L. Zhang, R. Lang, B. Qiao, Single-atom catalysis: bridging the homo- and heterogeneous catalysis, Chinese J. Catalysis 39 (2018) 893–898, https://doi.org/10.1016/S1872-2067(18)63047-5.
[15] C. Copéret, M. Chabanas, R.Petroff Saint-Arroman, J.-M. Basset, Homogeneous and Heterogeneous Catalysis: bridging the Gap through Surface Organometallic Chemistry, Angewandte Chemie International Edition 42 (2003) 156–181, https://doi.org/10.1002/anie.200390072.
[16] A. Wang, J. Li, T. Zhang, Heterogeneous single-atom catalysis, Nat. Rev. Chem. 2 (2018) 65–81, https://doi.org/10.1038/s41570-018-0010-1.
[17] F. Kraushofer, G.S. Parkinson, Single-atom catalysis: insights from model systems, Chem. Rev. 122 (2022) 14911–14939, https://doi.org/10.1021/acs.chemrev.2c00259.
[18] S.K. Kaiser, Z. Chen, D. Faust Akl, S. Mitchell, J. Pérez-Ramírez, Single-atom catalysts across the periodic table, Chem. Rev. 120 (2020) 11703–11809, https://doi.org/10.1021/acs.chemrev.0c00576.
[19] M.A. Bajada, J. Sanjosé-Orduna, G. Di Liberto, S. Tosoni, G. Pacchioni, T. Noël, G. Vilé, Interfacing single-atom catalysis with continuous-flow organic electrosynthesis, Chem. Soc. Rev. 51 (2022) 3898–3925, https://doi.org/10.1039/D2CS00100D.
[20] G. Di Liberto, S. Tosoni, L.A. Cipriano, G. Pacchioni, A few questions about single-atom catalysts: when modeling helps, Acc. Mater. Res. 3 (2022) 986–995, https://doi.org/10.1021/accountsmr.2c00118.
[21] C. Zhu, Q. Shi, S. Feng, D. Du, Y. Lin, Single-atom catalysts for electrochemical water splitting, ACS. Energy Lett. 3 (2018) 1713–1721, https://doi.org/10.1021/acsenergylett.8b00640.
[22] G.S. Parkinson, Single-atom catalysis: how structure influences catalytic performance, Catal. Letters. 149 (2019) 1137–1146, https://doi.org/10.1007/s10562-019-02709-7.
[23] H. Xu, Y. Zhao, Q. Wang, G. He, H. Chen, Supports promote single-atom catalysts toward advanced electrocatalysis, Coord. Chem. Rev. 451 (2022) 214261, https://doi.org/10.1016/j.ccr.2021.214261.
[24] G. Di Liberto, I. Barlocco, L. Giordano, S. Tosoni, G. Pacchioni, Single-atom electrocatalysis from first principles: current status and open challenges, Curr. Opin. Electrochem. 40 (2023) 101343, https://doi.org/10.1016/j.coelec.2023.101343.
[25] M.B. Boucher, B. Zugic, G. Cladaras, J. Kammert, M.D. Marcinkowski, T.J. Lawton, E.C.H. Sykes, M. Flytzani-Stephanopoulos, Single atom alloy surface analogs in Pd0.18Cu15 nanoparticles for selective hydrogenation reactions, Phys. Chem. Chem. Physics 15 (2013) 12187, https://doi.org/10.1039/c3cp51538a.
[26] G. Kyriakou, M.B. Boucher, A.D. Jewell, E.A. Lewis, T.J. Lawton, A.E. Baber, H. L. Tierney, M. Flytzani-Stephanopoulos, E.C.H. Sykes, Isolated metal atom geometries as a strategy for selective heterogeneous hydrogenations, Science (1979) 335 (2012) 1209–1212, https://doi.org/10.1126/science.1215864 (1979).
[27] M.D. Marcinkowski, M.T. Darby, J. Liu, J.M. Wimble, F.R. Lucci, S. Lee, A. Michaelides, M. Flytzani-Stephanopoulos, M. Stamatakis, E.C.H. Sykes, Pt/Cu single-atom alloys as coke-resistant catalysts for efficient C–H activation, Nat. Chem. 10 (2018) 325–332, https://doi.org/10.1038/nchem.2915.
[28] R.T. Hannagan, G. Giannakakis, M. Flytzani-Stephanopoulos, E.C.H. Sykes, Single-Atom Alloy Catalysis, Chem. Rev. 120 (2020) 12044–12088, https://doi.org/10.1021/acs.chemrev.0c00078.
[29] M.T. Greiner, T.E. Jones, S. Beeg, L. Zwiener, M. Scherzer, F. Girgsdies, S. Piccinin, M. Armbrüster, A. Knop-Gericke, R. Schlögl, Free-atom-like d states in single-atom alloy catalysts, Nat. Chem. 10 (2018) 1008–1015, https://doi.org/10.1038/s41557-018-0125-5.
[30] E.C.H. Sykes, P. Christopher, Recent advances in single-atom catalysts and single-atom alloys: opportunities for exploring the uncharted phase space in-between, Curr. Opin. Chem. Eng. 29 (2020) 67–73, https://doi.org/10.1016/j.coche.2020.06.004.
[31] P. Kress, R. Réocreux, R. Hannagan, T. Thuening, J.A. Boscoboinik, M. Stamatakis, E.C.H. Sykes, Mechanistic insights into carbon–carbon coupling on NiAu and PdAu single-atom alloys, J. Chem. Phys. 154 (2021), https://doi.org/10.1063/5.0048977.
[32] G. Giannakakis, M. Flytzani-Stephanopoulos, E.C.H. Sykes, Single-Atom Alloys as a Reductionist Approach to the Rational Design of Heterogeneous Catalysts, Acc. Chem. Res. 52 (2019) 237–247, https://doi.org/10.1021/acs.accounts.8b00490.
[33] M.T. Darby, M. Stamatakis, A. Michaelides, E. Charles, H. Sykes, Lonely Atoms with Special Gifts: breaking Linear Scaling Relationships in Heterogeneous Catalysis with Single-Atom Alloys, J. Phys. Chem. Lett. 9 (2018) 5636–5646, https://doi.org/10.1021/acs.jpclett.8b01888.
[34] C. Zhou, J.Y. Zhao, P.F. Liu, J. Chen, S. Dai, H.G. Yang, P. Hu, H. Wang, Towards the object-oriented design of active hydrogen evolution catalysts on single-atom alloys, Chem. Sci. 12 (2021) 10634–10642, https://doi.org/10.1039/D1SC01018B.
[35] M. Luo, J. Cai, J. Zou, Z. Jiang, G. Wang, X. Kang, Promoted alkaline hydrogen evolution by an N-doped Pt–Ru single atom alloy, J. Mater. Chem. a Mater. 9 (2021) 14941–14947, https://doi.org/10.1039/D1TA03593B.
[36] C. Chen, D. Wu, Z. Li, R. Zhang, C. Kuai, X. Zhao, C. Dong, S. Qiao, H. Liu, X. Du, Ruthenium-Based Single-Atom Alloy with High Electrocatalytic Activity for Hydrogen Evolution, Adv. Energy Mater. 9 (2019), https://doi.org/10.1002/aenm.201803913.
[37] J.K. Nørskov, T. Bligaard, J. Rossmeisl, C.H. Christensen, Towards the computational design of solid catalysts, Nat. Chem. 1 (2009) 37–46, https://doi.org/10.1038/nchem.121.
[38] G.J. Kubas, Molecular hydrogen complexes: coordination of a .sigma. bond to transition metals, Acc. Chem. Res. 21 (1988) 120–128, https://doi.org/10.1021/ar00147a005.
[39] G.J. Kubas, Fundamentals of H 2 Binding and Reactivity on Transition Metals Underlying Hydrogenase Function and H 2 Production and Storage, Chem. Rev. 107 (2007) 4152–4205, https://doi.org/10.1021/cr050197j.
[40] R.H. Crabtree, Dihydrogen complexes: some structural and chemical studies, Acc. Chem. Res. 23 (1990) 95–101, https://doi.org/10.1021/ar00172a001.
[41] R.H. Crabtree, Dihydrogen complexation, Chem. Rev. 116 (2016) 8750–8769, https://doi.org/10.1021/acs.chemrev.6b00037.

[42] G. Di Liberto, L.A. Cipriano, G. Pacchioni, Role of dihydride and dihydrogen complexes in hydrogen evolution reaction on single-atom catalysts, J. Am. Chem. Soc. 143 (2021) 20431–20441, https://doi.org/10.1021/jacs.1c10470.
[43] C. Saetta, G. Di Liberto, G. Pacchioni, Water Splitting on a Pt1/C3N4 single atom catalyst: a modeling approach, Top. Catal. (2023), https://doi.org/10.1007/s11244-023-01802-x.
[44] C. Saetta, I. Barlocco, G. Di Liberto, G. Pacchioni, Key Ingredients for the Screening of single atom catalysts for the hydrogen evolution reaction: the case of titanium nitride, Small. (2024), https://doi.org/10.1002/smll.202401058.
[45] I. Barlocco, G. Di Liberto, G. Pacchioni, Hydrogen complexes on single atom alloys: classical chemisorption *versus* coordination chemistry, Catal. Sci. Technol. 13 (2023) 5301–5312, https://doi.org/10.1039/D3CY00609C.
[46] M. Pineda, M. Stamatakis, Kinetic Monte Carlo simulations for heterogeneous catalysis: fundamentals, current status, and challenges, J. Chem. Phys. 156 (2022), https://doi.org/10.1063/5.0083251.
[47] R. Réocreux, M. Stamatakis, One Decade of Computational studies on single-atom alloys: is in silico design within reach? Acc. Chem. Res. 55 (2022) 87–97, https://doi.org/10.1021/acs.accounts.1c00611.
[48] M. Stamatakis, D.G. Vlachos, A graph-theoretical kinetic Monte Carlo framework for on-lattice chemical kinetics, J. Chem. Phys. 134 (2011), https://doi.org/10.1063/1.3596751.
[49] J. Nielsen, M. d'Avezac, J. Hetherington, M. Stamatakis, Parallel kinetic Monte Carlo simulation framework incorporating accurate models of adsorbate lateral interactions, J. Chem. Phys. 139 (2013), https://doi.org/10.1063/1.4840395.
[50] W. Li, S.E. Madan, R. Réocreux, M. Stamatakis, Elucidating the reactivity of oxygenates on single-atom alloy catalysts, ACS. Catal. 13 (2023) 15851–15868, https://doi.org/10.1021/acscatal.3c03954.
[51] G. Kresse, J. Hafner, Ab initio molecular dynamics for liquid metals, Phys. Rev. B 47 (1993) 558–561, https://doi.org/10.1103/PhysRevB.47.558.
[52] G. Kresse, J. Furthmüller, Efficiency of ab-initio total energy calculations for metals and semiconductors using a plane-wave basis set, Comput. Mater. Sci. 6 (1996) 15–50, https://doi.org/10.1016/0927-0256(96)00008-0.
[53] G. Kresse, J. Hafner, Ab initio molecular-dynamics simulation of the liquid-metal–amorphous-semiconductor transition in germanium, Phys. Rev. B 49 (1994) 14251–14269, https://doi.org/10.1103/PhysRevB.49.14251.
[54] J.P. Perdew, K. Burke, M. Ernzerhof, Generalized Gradient Approximation Made Simple, Phys. Rev. Lett. 77 (1996) 3865–3868, https://doi.org/10.1103/PhysRevLett.77.3865.
[55] P.E. Blöchl, Projector augmented-wave method, Phys. Rev. B 50 (1994) 17953–17979, https://doi.org/10.1103/PhysRevB.50.17953.
[56] G. Kresse, D. Joubert, From ultrasoft pseudopotentials to the projector augmented-wave method, Phys. Rev. B 59 (1999) 1758–1775, https://doi.org/10.1103/PhysRevB.59.1758.
[57] G. Henkelman, B.P. Uberuaga, H. Jónsson, A climbing image nudged elastic band method for finding saddle points and minimum energy paths, J. Chem. Phys. 113 (2000) 9901–9904, https://doi.org/10.1063/1.1329672.
[58] S. Grimme, J. Antony, S. Ehrlich, H. Krieg, A consistent and accurate ab initio parametrization of density functional dispersion correction (DFT-D) for the 94 elements H-Pu, J. Chem. Phys. 132 (2010) 154104, https://doi.org/10.1063/1.3382344.
[59] R.W.G. Wyckoff, Crystal Structures, Wiley, 1963.
[60] M.T. Darby, E.C.H. Sykes, A. Michaelides, M. Stamatakis, Carbon Monoxide Poisoning Resistance and Structural Stability of Single Atom Alloys, Top. Catal. 61 (2018) 428–438, https://doi.org/10.1007/s11244-017-0882-1.
[61] I. Barlocco, L.A. Cipriano, G. Di Liberto, G. Pacchioni, Does the Oxygen Evolution Reaction follow the classical OH*, O*, OOH* path on single atom catalysts? J. Catal. 417 (2023) 351–359, https://doi.org/10.1016/j.jcat.2022.12.014.
[62] S. Ravipati, G.D. Savva, I.-A. Christidi, R. Guichard, J. Nielsen, R. Réocreux, M. Stamatakis, Coupling the time-warp algorithm with the graph-theoretical kinetic Monte Carlo framework for distributed simulations of heterogeneous catalysts, Comput. Phys. Commun. 270 (2022) 108148, https://doi.org/10.1016/j.cpc.2021.108148.
[63] T. Ludwig, A.R. Singh, J.K. Nørskov, Subsurface nitrogen dissociation Kinetics in Lithium metal from Metadynamics, J. Phys. Chem. C 124 (2020) 26368–26378, https://doi.org/10.1021/acs.jpcc.0c09108.
[64] X. Zhang, G. Cui, H. Feng, L. Chen, H. Wang, B. Wang, X. Zhang, L. Zheng, S. Hong, M. Wei, Platinum–copper single atom alloy catalysts with high performance towards glycerol hydrogenolysis, Nat. Commun. 10 (2019) 5812, https://doi.org/10.1038/s41467-019-13685-2.
[65] H. Feng, M. Zhang, Z. Ge, Y. Deng, P. Pu, W. Zhou, H. Yuan, J. Yang, F. Li, X. Zhang, Y.-W. Zhang, Designing efficient single-atom alloy catalysts for selective C=O hydrogenation: a first-principles, active learning and microkinetic study, ACS. Appl. Mater. Interfaces. 15 (2023) 55903–55915, https://doi.org/10.1021/acsami.3c15108.
[66] M. Mavrikakis, J. Rempel, J. Greeley, L.B. Hansen, J.K. Nørskov, Atomic and molecular adsorption on Rh(111), J. Chem. Phys. 117 (2002) 6737–6744, https://doi.org/10.1063/1.1507104.
[67] M. Wijzenbroek, D. Helstone, J. Meyer, G.-J. Kroes, Dynamics of H2 dissociation on the close-packed (111) surface of the noblest metal: H2 + Au(111), J. Chem. Phys. 145 (2016), https://doi.org/10.1063/1.4964486.
[68] B. Jiang, H. Guo, Six-dimensional quantum dynamics for dissociative chemisorption of H_2 and D_2 on Ag(111) on a permutation invariant potential energy surface, Phys. Chem. Chem. Phys. 16 (2014) 24704–24715, https://doi.org/10.1039/C4CP03761H.
[69] F. Libisch, J. Cheng, E.A. Carter, Electron-transfer-induced dissociation of H_2 on gold nanoparticles: excited-state potential energy surfaces *via* embedded correlated wavefunction theory, Zeitschrift Für Physikalische Chemie (2013), https://doi.org/10.1524/zpch.2013.0406, 130708000310008.
[70] J. Schumann, Y. Bao, R.T. Hannagan, E.C.H. Sykes, M. Stamatakis, A. Michaelides, Periodic trends in adsorption energies around single-atom alloy active sites, J. Phys. Chem. Lett. 12 (2021) 10060–10067, https://doi.org/10.1021/acs.jpclett.1c02497.